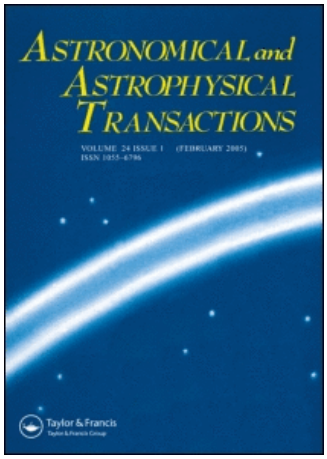

Astronomical & Astrophysical Transactions
The Journal of the Eurasian Astronomical Society
Publication details, including instructions for authors and subscription information:
http://www.informaworld.com/smpp/title~content=t713453505

Evolutionary regimes of the green-line corona brightness during cycles 20-21

O. G. Badalyan [a]; G. V. Kuklin [b]
[a] Institute of Terrestrial Magnetizm, Ionosphere and Radio-wave Propagation, Moscow region, Russia
[b] Institute of Solar-Terrestrial Physics, Irkutsk, Russia

Online Publication Date: 01 June 2000
To cite this Article: Badalyan, O. G. and Kuklin, G. V. (2000) 'Evolutionary regimes of the green-line corona brightness during cycles 20-21', Astronomical & Astrophysical Transactions, 18:6, 839 - 859
To link to this article: DOI: 10.1080/10556790008208178
URL: http://dx.doi.org/10.1080/10556790008208178

Astronomical and Astrophysical Transactions, 2000, Vol. 18, pp. 839–859
Reprints available directly from the publisher
Photocopying permitted by license only

EVOLUTIONARY REGIMES OF THE GREEN-LINE CORONA BRIGHTNESS DURING CYCLES 20–21

O. G. BADALYAN[1] and G. V. KUKLIN[2]

[1]*Institute of Terrestrial Magnetizm, Ionosphere and Radio-wave Propagation, 142092, Moscow region, Troitsk, Russia*
[2]*Institute of Solar-Terrestrial Physics, 664033, Irkutsk, Russia*

(Received November 2, 1998)

A non-standard approach to the interpretation of patrol green-line corona observations is presented. The brightness distributions in the years 1964–1986 (cycles 20–21) combined into half-year intervals and three latitudinal zones, were analysed using the statistical method of principal components. It has been determined that the variation of brightness distribution with cycle phase and latitude zone may be described by the so-called model of evolving distribution. Along the evolution trajectory four straight-lined parts are detected that are characterized by their own evolutionary regimes. The transitions from one regime to another take place at the specific (turning) points found from the cyclic curves of other activity indices (actually, the relative Wolf numbers). A 'latitude–time' diagram was constructed to show the time development of these regimes. Similar features of cycles 20–21 in this diagram, as well as the differences between the even and odd cycles are described. The physical meaning of these phenomena is briefly discussed.

KEY WORDS Sun: corona, green coronal line, statistical data analysis, cycles of activity

1 INTRODUCTION

The emission of the green coronal line λ 530.3 nm Fe XIV originates mainly in structural formations of the inner corona at a temperature of $\sim 10^6$ K and a density of $(1\text{–}2)\times10^9$ cm^{-3}. The basic structures of the inner corona are arches of various sizes – magnetic tubes filled with dense hot plasma. Under the influence of magnetic fields, individual tubes merge to form structures of larger size.

Observations of the green-line corona with a narrow pass-band filter reveal its pronounced inhomogeneity and dynamical changes. One can detect coronal condensations above active regions, high loops above quiet prominences, arches linking the neighbouring active regions, flare loops, and other features. Large-scale phenomena, such as coronal holes and coronal mass ejections, are also observed in the

green line. A variety of coronal structures reflects the existence of magnetic fields of different temporal and spatial scales – from small-scale to global background fields.

It is obvious that the green-line corona brightness observed at the limb is the integral (total) brightness of all features located along the line of sight. Different structural features of the solar corona are characterized by the brightness values within their own limits. The brightness values of these features display different dependencies on the height and, probably, on the phase of the cycle. Since every type of coronal feature can be characterized by its own distribution of brightness, the observed total distribution of the green-line corona brightness may contain, in explicit or implicit form, information about these coronal features, their physical nature and behaviour depending on the phase of the cycle and the heloigraphic latitude.

Systematic routine observations of the green coronal line began in 1943 at the Pic-du-Midi Observator. These observations were later continued on the world network of coronal stations, and at present they cover about five 11-year solar cycles. The accumulated data allow a detailed statistical analysis.

A study of variations in the green-line corona during an activity cycle was undertaken by Waldmeier (1955), who showed that two zones could be detected in the latitudinal distribution of the green-line corona brightness – the main and the polar zones. According to Waldmeier (1955), the main zone is most closely related to faculae whereas the polar zone shows no obvious connection with any photospheric or chromospheric manifestations of activity. Later, a large number of investigations of the green-line corona brightness distributions were carried out with respect to the latitudinal and longitudinal variations during the activity cycle, and the north–south asymmetry, and comparisons were made with other solar activity indices (see, for example, Sýkora (1980), Leroy and Noëns (1987), Bumba *et al.* (1990), Sýkora (1992) and references therein). Bumba *et al.* (1990) carried out a detailed comparison of the green-line corona brightness in two latitudinal zones separated at $\varphi = \pm 45°$, with sunspots, with the number and the total area of prominences, with polar faculae, and with photospheric magnetic fields during cycles 20–21. Sýkora (1992) investigated variations of the green line intensity over the whole period covered by the observations (about 4.5 activity cycles) for different latitudinal zones. Later this work was continued (see Storini and Sýkora, 1997).

In all the quoted papers the brightness values were examined directly. In our paper, we would like to offer a non-standard approach to the interpretation of patrol observations of the green coronal line. Rather than dealing with the intensity values we have used histograms of the numbers of records in certain intensity ranges during the given time interval – in other words, the distributions of the intensity values.

The goal of this paper is to study regularities in the change of distributions of the green coronal line intensities. When processing observational data for cycles 20–21 we have applied the statistical principal component analysis (PCA) in order to detect two or more typical distributions corresponding to various structural features of different physical nature in the corona. As a result we have obtained four types of distributions; these types evolve from one to another depending on the phase of the cycle and on heliolatitude, which means a change of different regimes in the

ordering of coronal structures with time and latitude. The analysis revealed both the regularities common for cycles 20–21, and the distinctions between the odd and even cycles. The preliminary results for cycle 21 were published by Badalyan *et al.* (1993), and Badalyan and Kuklin (1993).

2 OBSERVATIONAL DATA

We used observational data series of the green-line corona brightness during the years 1964–1986 (cycles 20–21). These are the patrol observations performed at a small world network of coronal stations.

The available observational data are extremely inhomogeneous. The data from each station have their peculiarities which make direct statistical analyses difficult. The problem of combining all these data to form a common non-contradictory system is very complicated. Some aspects of this problem were considered by Sýkora (1971, 1992). Here, we have used the observational data combined into a common system with the Lomnicky Štit data as the main reference series. The tabulated data have been partly published by Rybanský *et al.* (1989, 1990, 1991). The unpublished data were provided by courtesy of Drs. V. Rušin and M. Rybanský who made them available to us in computer format. The procedure of data homogenization is described by Rybanský (1975) and Rybanský *et al.* (1985).

The tabulated values of the green line intensities are expressed in absolute coronal units, i.e. in millionths of the brightness of the solar disk centre in 1 Å interval of the neighbouring continuum, and are reduced to the height at 40″ above the limb. During the observations, measurements were made around the whole solar disk with a 5-step in the position angle (72 points along the limb). Using the data from a network of coronal stations one can have about 280 observational days per year. The missing days were interpolated in tables by Rybanský *et al.* (1989, 1990, 1991), but here we have omitted the interpolated values.

In our analysis, the observational data were grouped into half-year intervals and three latitudinal zones (in practice this means the position angles, and we have then made corrections due going from the position angle to the heliographic latitude for each season, see Appendix 2): the equatorial zone – from 0° to ±20°, the middle-latitude zone – from ±25° to ±50° and the polar zone – from ±55° to ±90°. So, we have combined the northern and the southern hemispheres. This does not permit us to study the N–S asymmetry but shows more clearly the latitude dependence of the distributions under consideration. The boundaries of the latitudinal zones were selected by proceeding from the following considerations: the lower boundary of the middle-latitude zone roughly corresponds to the boundary of the sunspot formation zone, and the upper boundary coincides with the region of quiecent prominences.

We should like to emphasize that we do not deal with the real brightness values. Inside each half-year interval and latitudinal zone, the number of data points was counted in which the values of the green coronal line intensity fall into the interval of 0–9 absolute coronal units (a.c.u.), 10–19 a.c.u., etc., to 190–199 a.c.u.; in all, we have 20 intensity intervals. The small number of cases, when the intensity exceeds

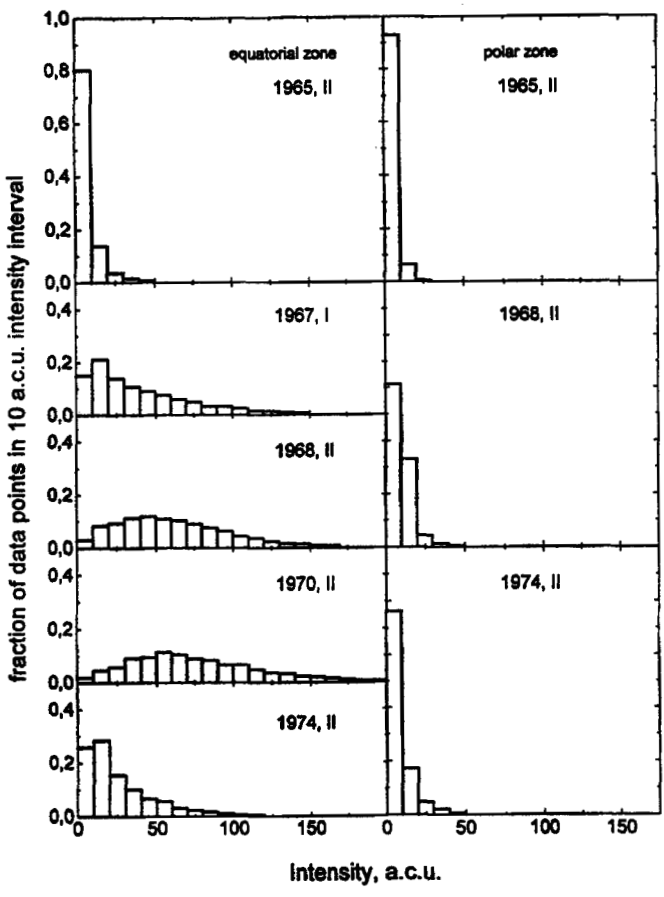

Figure 1 Examples of initial normalized intensity distributions for different cycle activity phases and latitude zones. Intensity is given in absolute coronal units (a.c.u.).

200 a.c.u., has been omitted from this paper; they are considered to be probably due to powerful non-stationary phenomena in the solar corona and are not relevant to the slowly varying quiet corona. Since they are rare, neglecting them does not affect our results. Therefore, we obtain the initial brightness distributions, six of them for each year.

In Figure 1 we present some histograms of the green-line corona brightness distributions for the equatorial and polar zones and for different phases of cycle 20. As seen from Figure 1, the small brightness values are dominant at the beginning of the cycle. Later, the histogram maximum shifts step by step to larger values and diminishes in height – the dispersion increases and the distribution curve widens. After the cycle maximum is passed, the histogram changes reverse. The largest amplitude of variations in the brightness distributions is observed in the equatorial

zone, while in the polar zone the changes are small. In Badalyan *et al.* (1993) and in Badalyan and Kuklin (1993), examples of histograms for cycle 21 are presented, as well as the dependence of the average brightness and the corresponding dispersion on the cycle phase.

The totality of all distributions so obtained enables us to form a matrix P, where the rows are the above-mentioned distributions and each row corresponds to a certain half-year and a latitudinal zone. Therefore we have 138 rows, i.e. 46 half-years × 3 latitudinal zones. Sums along the rows (sample values), which mean the total number of observations for a given time interval and latitudinal zone, are in the range 1150–4650. The matrix formed in this way is a database for the following mathematical and statistical treatment.

3 PRINCIPAL COMPONENT ANALYSIS AND THE RESULTS OF ITS APPLICATION TO THE DATA OF CYCLES 20–21

PCA basically consists in finding eigenvectors (principal components) in terms of which the obtained initial intensity distributions can be expanded. Three cases can be distinguished: (1) the total distribution is a mixture (a linear combination) of some typical distributions with constant parameters; in this case, the obtained partial distributions describe different physical objects, and contributions (shares) of these distributions in samples depend on the cycle phase and the latitude; (2) at certain moments, a sharp transition from one typical distribution to another takes place; (3) there is a single distribution, whose parameters evolve with time and also depend on the latitude.

For these three possible cases, we have to expect entirely definitive relations between the coefficients C_m^{jk}. In the case of a linear combination of typical distributions (a mixture), in a space where the coordinates are the coefficients C_m^{jk} corresponding to each input distribution, the imaging points must concentrate close to a straight line, a plane or a hyperplane passing through the points that represent 'pure' typical distributions. If there is not a mixture of typical distributions but sharply pronounced transitions from one distribution to another depending on cycle phase and/or latitude, then the imaging points will be gathered in compact clusters around the points, corresponding to the standard distributions. The coordinates of the centres of gravity of these clusters are the coefficients of the principal component expansion for the desired typical distributions. This case exemplifies the solution of the problem of automatic classification of distributions with the help of principal component analysis, and it is widely used in the problem of pattern recognition. And finally, in the case of an evolving distribution which depends (non-linearly, as a rule) on changing parameters, the imaging points are to be located close to some curve, surface or hypersurface. These three possible cases are shown schematically in Figure 2, where a projection of imaging points on the C_1C_2 plane is given.

In our case the principal component expansion of a set of 138 initial distributions $n(I)$ has the form

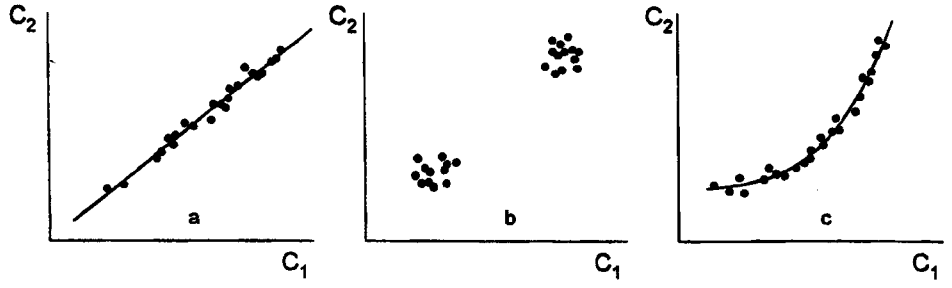

Figure 2 Scheme illustrating the relative disposition of imaging points for the following cases: (*a*) a linear combination of typical distributions; (*b*) abrupt transitions from one distribution to another; (*c*) an evolving distribution.

$$n_{jk} = n(I; t_j, \varphi_k) = \sum_m C_m(t_j, \varphi_k)\nu_m(I)\,. \tag{1}$$

Here $\nu_m(I)$ are the eigenvectors (principal components) of the matrix Q, numbered in order of decreasing eigenvalues; and the coefficients $C_m^{jk} \equiv C_m(t_j, \varphi_k)$ describe the contributions of these components to individual distributions (realizations). The j and k indices refer to the half-year number ($1 \leq j \leq 46$) and the latitude zone number ($1 \leq k \leq 3$) respectively; the m index indicates the number of expansion terms we need for an adequate description of the individual distributions. The computed eigenvectors of the matrix Q and the expansion coefficients, C_m^{jk}, are the material we have to use in order to find the typical distributions we are interested in, if any. A short description of the PCA is given in Appendix A.

As in an earlier paper (Badalyan and Kuklin, 1993), the initial distributions were transformed a little to arrange computations in a more convenient way: (1) to make the elements of the matrix Q not too different in magnitude, each distribution $n_{jk}(I_i)$ (identical to a probability density function) was replaced by a cumulative sum $N_{jk}(I_i) = \sum_{l=1}^{i} n_{jk}(I_l)$, analogous to an integral distribution function; (2) in order to have full correspondence and homogeneity, the obtained $N(I)$ were normalized by dividing them by the number of measurements (a sample size) in a given half-year and a given latitude zone. These values were used to form the matrix P (138×20), all elements of which satisfy the condition $0 < p_{jk} < 1$.

The transposed matrix, P^T (20×138), is formed, then the autocovariation matrix, Q (20×20), is calculated, and the eigenvectors, ν_m, of the matrix Q and the coefficients C_m^{jk} are found. Now our distributions can be presented in the form (1) with the obtained coefficients and eigenvectors.

It turned out that five expansion terms were enough to solve our problem. Besides, the first three of them describe more than 99.5% of the total dispersion. In more exact terms, the sum of eigenvalues of these components constitutes more than 99.5% of the sum of all eigenvalues of the matrix Q. The error caused by

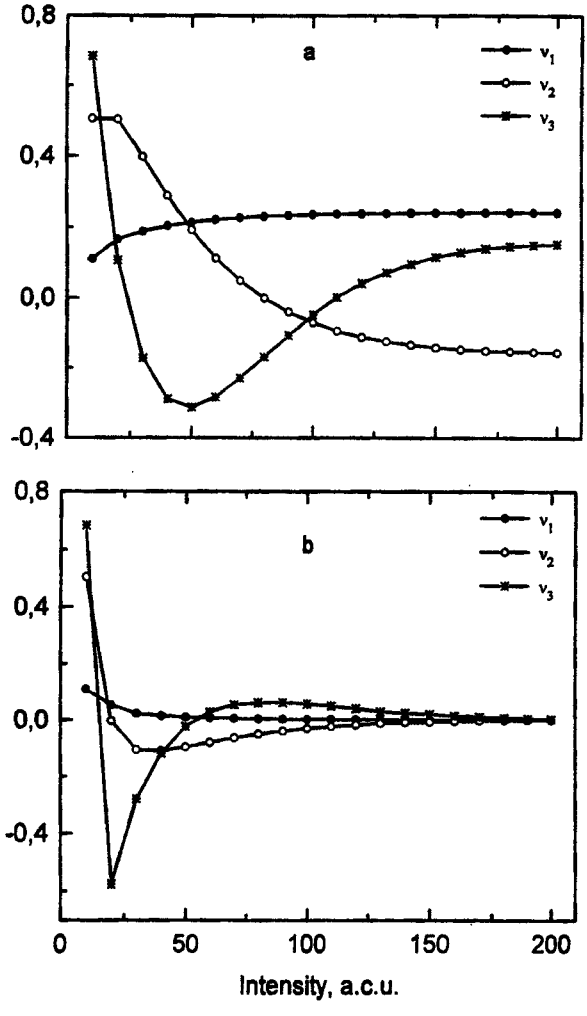

Figure 3 The first three principal components (eigenvectors), ν_1, ν_2, and ν_3 for the cumulated sums (*a*) and for the initial normalized distributions (*b*).

neglecting the remaining expansion terms does not exceed the statistical accuracy of the original data, i.e. 2–4%.

Figure 3 illustrates the first three principal components (eigenvectors), ν_1, ν_2 and ν_3, that are the natural basic functions for describing each of the 138 intensity distributions as a linear combination of these functions. Here, ν_1 represents the most common part of all the initial distributions, ν_2 the most typical deviations from the common part, and ν_3 the individual variations of the deviations. The

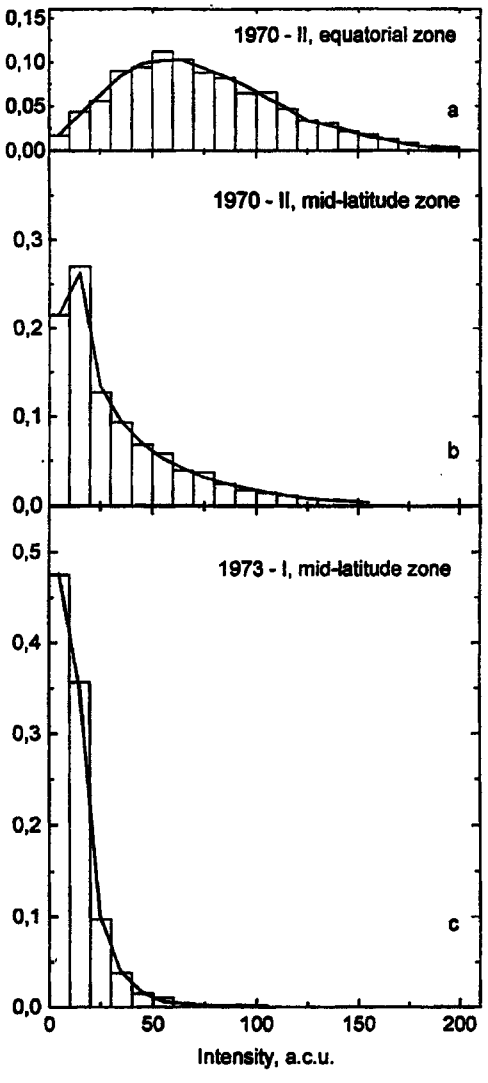

Figure 4 Examples of the representation of the initial intensity distributions in the form of expansion (1). The distributions shown refer to the evolutionary regimes A (a), B (b), and C (c).

vectors in Figure 3a correspond to the solution for the cumulative sums, the vectors in Figure 3b for the initial normalized distributions (see Figure 1). Each of the vectors in Figure 3b is included into the expansions of the initial distributions with a weight equal to the corresponding coefficients C_1, C_2, C_3.

Figure 4 gives three examples of the representation of the initial intensity distributions by expansion (1). To plot these curves, we used the vectors represented

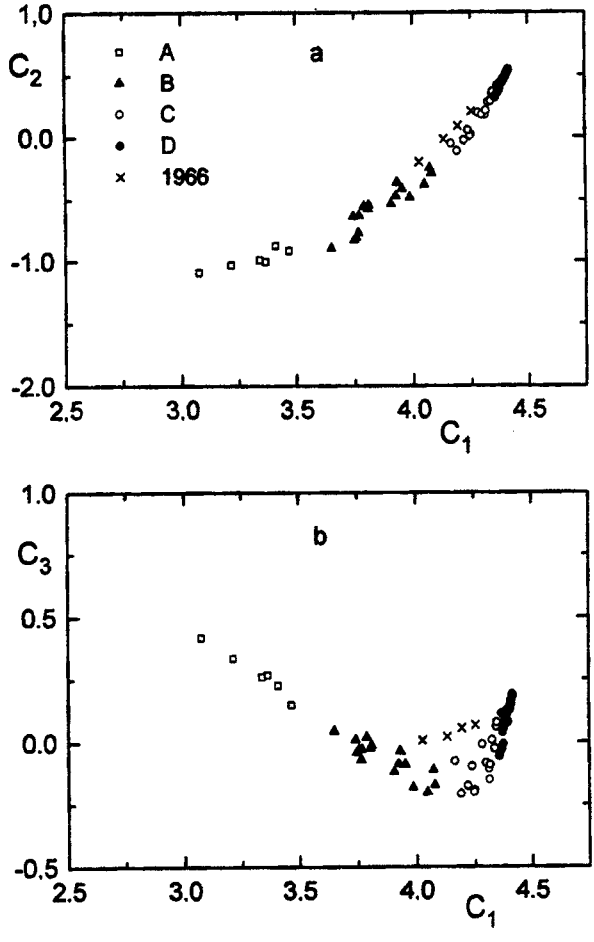

Figure 5 The computed coefficients of the principal components expansion for cycle 20. Four regimes on the evolution trajectory are indicated.

in Figure 3*b*. Four expansion terms describe the initial distribution practically exactly; in the limits of statistical scattering, three expansion terms are almost always sufficient. The histograms in Figures 4*a*, 4*b*, 4*c* refer to the evolutionary regimes A, B, C, respectively (see below).

So, we then consider three first coefficients C_m ($m = 1, 2, 3$), for each row of the matrix P, that is for each initial distribution (from here on we omit the indices jk for convenience). These coefficients can be represented as coordinates of the imaging points in the three-dimentional space $C_1C_2C_3$ – the space of distribution types.

The results of computations are presented in Figure 5 (cycle 20, years 1964–75) and in Figure 6 (cycle 21, years 1976–86). Projections of the whole totality

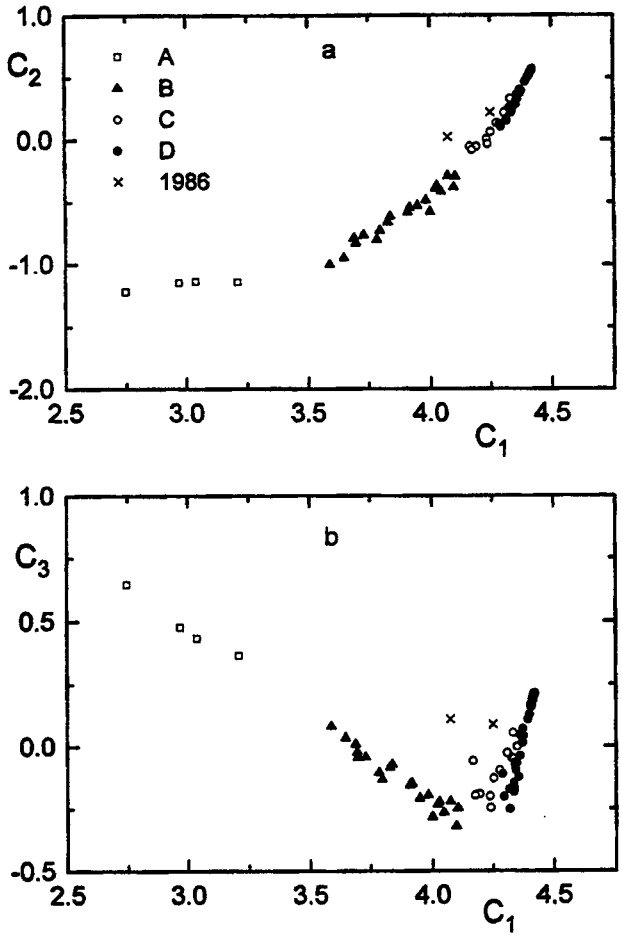

Figure 6 The same as in Figure 5 for cycle 21.

of imaging points on to the C_1C_2-plane are given in Figures 3*a* and 4*a*, and on the C_1C_3-plane in Figures 3*b* and 4*b*. The C_m coefficients, presented in Figures 3 and 4 and corresponding to each imaging point, numerically describe the kinds of changes of the green-line corona brightness distributions depending on cycle phase and latitude zone. (Notice, that we showed the $-C_3$ coefficient in Figure 3*b* in Badalyan and Kuklin, 1993.)

The computations made here for the 23-year data series confirm the results obtained by us earlier (Badalyan and Kuklin, 1993). As in the case of previous computations, made only for the years 1977–86, the imaging points in Figures 3 and 4 lie in the limits of comparatively narrow curvilinear bands, which means they form something like a 'tube' in the 3-D space $C_1C_2C_3$. We must emphasize that all

138 imaging points are arranged inside a single 'tube' and, only for convenience of description and analysis, have we represented them as separate plots for each activity cycle. Therefore, the conclusion we made earlier is confirmed: we cannot detect types of standard distributions. So, the obtained results should most preferably be interpreted as the existence of an evolving distribution (see Figure 2).

One can see that for both cycles (as earlier we have obtained results only for cycle 21 (Badalyan and Kuklin, 1993) the imaging points fall in bands disintegrated into sections with gaps between them. Again we can isolate stretches A, B, and $C + D$, which can be identified in both projections. The stretch C branches off the stretch D, and this separation may be performed only on the C_1C_3-plane projection. All four stretches may be well approximated with straight-line segments. This means that their specific types of distribution, own evolutionary regimes exist in the limits of each of these parts.

By superimposing Figure 5 on Figure 6, one can see that the approximating straight lines are almost the same for stretches C and D in both cycles. There are, however, noticeable distinctions for stretch B and especially for stretch A. In particular, the gap between these stretches corresponds to different values of the C_1 coefficient in cycles 20 and 21. Perhaps this discrepancy is caused by the difference between the even and the odd cycles.

We would like to note the following fact. There are some points falling outside the general regularity in Figures 5 and 6 (they are marked by triangles). These points correspond to the equatorial and mid-latitude zones in the year 1966 (four points in Figure 5) and the equatorial zone in the year 1986 (two points in Figure 6). It is interesting that these points belong to the epoch of the transition from odd to even cycles. It would be useful to clarify whether this fact is regular, or is conditioned by the database used.

The population of the stretches corresponding to four evolution regimes is not at all casual. Stretch D contains the points belonging to the polar zone during all cycle phases. We include in it some points of the mid-latitude and equatorial zones in the epoch of solar activity minima (the years 1964 and 1976). The right-hand edge of stretch D corresponds to the cycle phases of low activity (large values of C_1), and the left-hand one corresponds to the maximum phase. Generally, the solar activity increase corresponds to diminishing C_1 coefficients and to the leftward shift in all stretches, and, on the contrary, the shift along the bands takes place in the opposite direction during the descending phase of solar activity.

The points populating stretch C belong to the mid-latitude zone at the low-activity phase and to the equatorial zone during the lowest activity, closely before and after the minimum. Stretch B contains the points of the mid-latitude zone during the high-activity phase and the points belonging to the low-latitude zone during the intermediate activity phases. Finally, stretch A contains only the points of the equatorial zone during the maximum cycle epoch: six points of cycle 20 (the years 1968–70) and four points of cycle 21 (the years 1981 and 1982).

Therefore, the evolution trajectories of three latitudinal zones may be described in the following way. In the low-latitude zone the evolution of the original distributions takes place along a regime sequence D–C–B–A–B–C–D; in the middle-

latitude zone along the regime sequence D–C–B–C–D; and in the polar zone the points imaging the source distributions never leave regime D.

4 'LATITUDE–TIME' DIAGRAM OF THE EVOLUTIONARY REGIMES AND THE RELATION TO THE TURNING POINTS OF THE WOLF NUMBER CYCLIC CURVE

Since the four stretches of the evolution trajectory may be approximated by straight-line sections, it is convenient to choose the C_1 coefficient as a basic parameter for describing the whole picture of the evolution of brightness distributions. Then the C_2 and C_3 coefficients may be easily defined as linear functions of C_1 and, obviously, these functions are different for each part. As shown above, the parameter C_1 changes with cycle phase and latitude zone, and it decreases with activity growth and from high to low latitudes. This allows us to construct a detailed 'latitude–time' diagram for the C_1 and then to determine on this diagram the locations of regions occupied by the evolutionary regimes corresponding to the A–D stretches. These regimes are symbolized by the same characters.

As pointed out above, the original data were divided into three latitudinal zones, and both hemispheres, the northern and the southern ones, were combined. Therefore, to represent the dependence of the C_1 coefficient on time and latitude, we have chosen an expansion whith respect to even powers of $\sin\varphi$, where φ is a heliographic latitude (roughly estimated by the position angle of measurement):

$$C_1(t,\varphi) = g_0(t) + g_2(t)\sin^2\varphi + g_4(t)\sin^4\varphi\,. \tag{2}$$

The $g_0(t)$, $g_2(t)$, and $g_4(t)$ values were computed for each half-year. Then each of these functions was approximated by a modified cubic spline (see Appendix B for details). Finally, the interpolation of the C_1 coefficients was carried out over the grid $\Delta\varphi = 5$–$10°$ and $\Delta t = 1.5$–3 months.

Now, the boundary values of C_1 (separating the stretches of different evolutionary regimes) need to be determined to reveal the corresponding areas on the latitude–time diagram. However, as it became clear, appropriate approximating straight lines do not intersect in the 3D space $C_1C_2C_3$, but pass close to one another. This is the reason why we have preferred to determine the boundary values of C_1 as the mid-points between the edges of the neighbouring stretches (the same coordinate values for cycles 20 and 21, that is all imaging points are combined): $C_1^{AB} = 3.5584$, $C_1^{BC} = 4.1166$. The right edge of the stretch C corresponds to a point of branching, or its intersection with the stretch D (roughly in the middle of the stretch D), i.e. $C_1^{CD} = 4.3686$. One can see that the greatest portion of the stretch C overlaps with the stretch D in the projections onto the C_1-axis and so these regimes cannot be separated using the parameter C_1. This is why we have taken the point $C_1^{BD} = 4.1962$, located in the middle between the edges of stretches B and D, as an arbitrary left edge of the stretch D.

The resulting latitude–time diagram is given in Figure 7, where the locations of the four regimes are shown. The areas are marked $C + D$ where both regimes C and

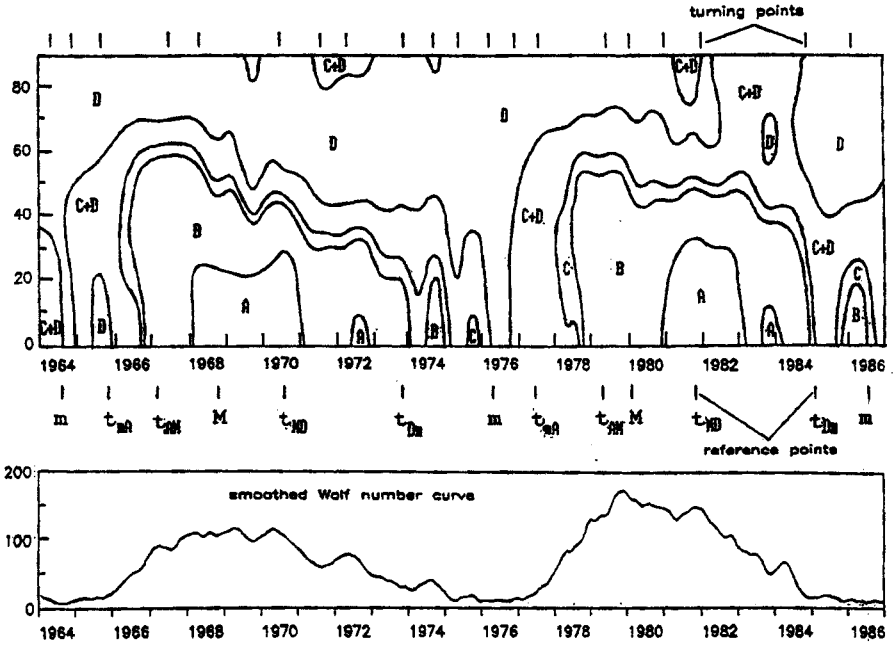

Figure 7 Latitude–time diagram for cycles 20–21. The locations of the regimes A–D are shown.

D may be observed simultaneously. It is apparent that the areas must be identified as the areas of the C-regime where the condition $C_1^{BC} < C_1 < C_1^{BD}$ is satisfied. We can see that the diagram contains a lot of detail whose existence was unimaginable using only the averaged original distributions: for example, regime D at latitudes $\varphi = 60°$–$70°$ during maximum activity or short-time inclusions of regimes A and B at the ends of the cycle.

In the lower panel of Figure 7 we present the cyclic curve of Wolf numbers for the time interval considered and mark the locations of the reference points according to the modern scenario of an 11-year solar activity cycle (Kuklin *et al.*, 1990; see Appendix C). We see that the cardinal changes of the evolutionary regimes with latitude take place roughly at the moments marked 'reference points'.

The time development of the whole pattern may be described in the following way. At cycle start (the epoch of minimum activity) the polar corona (regime D) extends over all latitudes down to the equator. After the beginning of the ascending phase (the reference point t_{mA}) regime B appears in low latitudes and reaches its highest latitudes ($\approx 60°$) at the beginning of the maximum phase (the reference point t_{AM}). After the maximum the high-latitude border of regime B drifts to latitudes 45°–50° (the quiescent prominence zone) where it remains till the end of the descending phase (the reference point t_{DM}) and later goes to the equator. Its place in low latitudes is occupied by regime $C + D$, and the polar corona (regime

D) again extends down to $\approx 40°$ latitudes. Regime A, the active equatorial corona, arises in low latitudes ($|\varphi| \leq 30°$) at the polarity reversal epoch or a little earlier and exists approximately till the middle of the descending phase. In our opinion, this regime is related to the existence of large complexes of activity with large bright coronal structures above them, extending in area and in height.

In Figure 7 we also see other details intrinsic to both cycles, among which one can indicate consecutive bursts of regimes A, B and C in the equatorial zone during the descending phase and invasions of regime $C + D$ near the pole after maximum activity.

Differences between even and odd cycles may also be indicated. In odd cycle 21 the influence of regime C after the maximum is stronger and causes the merging of the polar area with the middle-latitude one, occupied with the same regime. The shorter lifetime of regime B in cycle 21 in comparison with cycle 20 is also noticeable.

As mentioned above, the reference points approximately mark the changes of the evolutionary regime locations on the latitude–time diagram. Keeping this fact in mind, we have also compared our diagram with the positions of the turning points of the Wolf number cyclic curve (the points where the derivative changes sharply), determined by Kuklin (1992). We can see that many fine details of the latitude–time diagram correspond to the locations of the turning points. We suppose as a very essential fact that global changes of evolutionary regimes of the green-line corona brightness distributions are connected with the reference and turning points that are determined using low-latitude sunspot activity. Badalyan and Kuklin (1993) made the comparison of drastic changes on the latitude–time diagram of cycle 21 with essential longitudinal arrangements of the low-latitude background magnetic fields, which also shows some conformity.

5 POSSIBLE INTERPRETATION OF THE LATITUDE–TIME DIAGRAM

The latitude–time diagram shows the distribution and the shift of different evolutionary regimes of the green-line corona brightness on the solar surface depending on the phase of the cycle. This diagram reflects the behaviour and the time ratio of magnetic fields of different scales: large-scale fields determining the shape of the corona and its large features, and local ones, responsible for bright coronal condensations and aggregates of arch elements. At the solar maximum local magnetic fields occupy a significant area on the solar surface. At this time, the green-line corona brightness is determined by the regimes A and B, whereas the regime D occupies only a small area in the polar region. After the polarity reversal, in accordance with the changes in the correlations between fields of different scales (for local fields those are well-known Maunder butterflies; the large-scale fields have been investigated in many papers, see, for example, Hoeksema, 1991), the regime D gradually penetrates to low-latitude regions of the corona, replacing the regimes A and B connected with local fields. Bursts of A and B regimes at the end of the cycle appear to be precursors of the next cycle (Obridko and Gaziev, 1992).

Comparing our latitude–time diagram to the maps of the green-line corona brightness isolines (Sýkora, 1994) we see a correspondence between the coronal brightness and the locations of our evolutionary regimes. According to this idea, the regimes A and B are bright loops above active regions, the brightest regime A probably reflecting the integration of arch elements into structures of large size by large-scale magnetic fields. Near the minimum the faint background corona of the polar regions (regime D) fills all latitudes; the A and B regimes disappear.

The results obtained may be interpreted in terms of the following model. In active regions of the low-latitude zone the green-line corona emission is connected with bundles of thin magnetic arches with roughly the same physical parameters, density and temperature. The brightness of the corona at a given point on the plane of the sky depends on the number of these elements along the line of sight and on their brightness, that is, on the number of arches per area unit and on the arch distribution with respect to their heights. The existence of the band in Figures 3 and 4 joining the points of the low-latitude zone in the activity maximum and points of the high-latitude zone at any activity level (the evolution peculiarity), is evidence, in our opinion, in favour of the fact that these arch elements are the same (in terms of physical conditions in them) over the whole Sun and during all cycle phases. The variations of the brightness distributions considered here result from changes of the number, spatial distribution and brightness (they may probably be connected with their geometric sizes) of these elements, depending on cycle phase and latitude. Hence we can speak about the uniformity of the 'construction details' or 'bricks' (that is, of the arch elements) which form more complicated structures.

6 DISCUSSION

Therefore, the application of principal component analysis to the totality of the green-line corona brightness distributions in cycles 20–21 (the years 1964–86) permits us to describe quantitatively the character of the changes of these distributions with time. We arrive at the conclusion that the considered observational data may be treated in terms of one evolving distribution. The totality of points, imaging source distributions (the expansion coefficients), form a bent tube in the 3D space $C_1C_2C_3$. In the projection of this tube onto the planes C_1C_2 and C_1C_3 one can distinguish four straight-line parts which correspond to different latitudes and various levels of coronal activity. In the limits of these parts, the intrinsic evolutionary regimes of the distributions of the green-line corona brightness occur during consecutive cycle phases. For each of the three latitudinal zones the evolution of the initial distributions proceeds with a different amplitude: in the equatorial zone the process covers the whole evolution curve, in the middle-latitude zone it is in the limits of some part of this curve, whereas in the polar zone the source distributions change only in the limits of a small section of the evolution trajectory.

The constructed latitude–time diagram, where the positions of the regions occupied by the four evolutionary regimes are shown, testifies that the changes of the evolutionary regimes take place at moments (singular points of the cycle) detected

with the use of indices describing processes in the sunspot formation zone. Such an accordance, in our opinion, indicates that changes in the overall structure and ordering of the arch elements over the whole Sun, on the one hand, and the behaviour of the small-scale, local and global magnetic fields, on the other, can be described in terms of a single scenario. Today we cannot yet imagine clearly all regularities and physical causes of this phenomenon. Nevertheless this conclusion seems to us to be the most essential one.

We should like to note that the results obtained here need further confirmation on closer examination of the observational data.

7 APPENDIX A

Here, we describe briefly the statistical method used to analyse the obtained initial distributions. The method permits us to quantitatively describe the changes in the distribution of brightness as a function of the activity cycle and heliolatitude.

The method of principal components, which we are using, is an old and well-known tool of multidimensional analysis. Similar ideas were proposed by K. Pearson (1901) at the very beginning of the twentieth century. Later they were developed in detail by Hotelling (1933) and were used by Karuhnen (1947) and Loewe (1963) in creating the concept of canonical expansion in the theory of stochastic processes. The method was widely used in many areas of physics and astrophysics, including the statistical studies of solar activity (e.g. Wertlieb *et al.*, 1971); Kuklin (1980) applied principal component analysis to the problem of two populations of sunspot groups. Unfortunately, today this technique is poorly known among most solar physicists, though it is expounded in many textbooks on statistical processing of multidimensional data (Wilks 1962, Rao 1965, etc.).

Principal component analysis (PCA) is a generalization of the well-known method of superposed epochs, suggested by Cree. Assume that we have measurements of some value, A_{tp}, depending on two parameters, t_i and p_k, where $i = 1, \ldots, n$ and $k = 1, \ldots, m$ (e.g., long time series of the same value measured at different points of space). Let us form a matrix, P, consisting of $m \times n$ elements. In this case, the rows can be considered as n realizations of a random value, A_t, depending on the paramter p_k, and the columns as m realizations of a random value, A_p, depending on the parameter t_i. In the Cree method, the matrix elements must be averaged over each column (or over each row) in order to obtain a mean realization that is regarded as the main common component in each realization. The contribution of this common component to each realization may vary in a regular way from one realization to another. Moreover, there may exist some other components also varying regularly, but in different ways and making weaker contributions. The mean realization, determined in the Cree method, may depend linearly on these other components.

Let us consider for definiteness the matrix, $P(m \times n)$, of realizations of the random value, A_t, depending on the parameter p_k. PCA permits us to find n such components unambiguously assuming them to be orthogonal, i.e. linearly

independent, and to estimate their amplitude variations from one realization to another. Usually, the number of physically significant components, l, is less than n, and the rest describe small contributions of various non-correlated stochastic (noise) components. It is possible to restrict the PCA expansion procedure by a given number of components, l' (the case of factor analysis), but the choice of l' and the estimation of the components become ambiguous.

Now we describe the PCA procedure briefly. The data matrix, $A(m,n)$, must be converted into an autocovariance matrix, $B(n,n) = A^T A$ (we consider the case $m > n$) or an autocorrelation matrix $R(n,n)$. Further, we need to solve an eigenvalue problem for B or R. The solutions must be arranged in order of decreasing eigenvalues, λ_k (and eigenvectors x_k must be ordered similarly).

The totality of eigenvectors of the matrix, Q, is the basis of the principal components for the input matrix, P, to expand the initial individual realizations (rows). This basis is not constructed *a priori*, but is based on the input information, so that it may be called a basis of natural orthogonal functions. The expansion is economical and mean square in the following sense. If we arrange the eigenvectors (the principal components) in decreasing order of the corresponding eigenvalues of the matrix, Q, then certain first terms describe the main part of the information contained in the matrix, P. In other words, it is not necessary to use all terms of the expansion, and this truncated expansion provides a minimum mean square error of the data presentation. The first terms of the expansion involve information about the main general features of realizations, whereas the noise and individual peculiarities are 'transferred' to the higher-order expansion terms. Usually, in the case of 'good' data (with a small contribution of noise and individual peculiarities to the total dispersion) the first 2–4 expansion terms can describe up to 90–98% of the total dispersion. Generally, the first eigenvector presents the most common part of all initial distributions; the second one, the most typical deviations from the common part; and the third one, the characteristic variations of deviations, etc.

Further analysis can be carried out in terms of relationships between different components. It should be noted that the determined principal components are in some sense *abstract* mathematical images. So, after being obtained, the regularities have to be described in terms of physical or astrophysical concepts. But at intermediate stages of the PCA interpretation, it is necessary to focus attention on the mathematical (geometrical) search for regularities for the objects not directly adequate to our customary concepts.

8 APPENDIX B

In order to construct a latitude–time diagram with the expression (2), an interpolation of the function $C_1(t,\varphi)$ is required. The computations made in accordance with the principal component method give us the matrix of discrete values of coefficient C_1 for N ($N = 46$) half-year intervals and three latitudinal zones. As we want to represent the required function as (2), so the computed coefficients for each

latitudinal zone must be written as

$$C_{i,k} = 2G_{0,k} \int_{\varphi_1}^{\varphi_2} \mathrm{d}\varphi + 2G^*_{2,k} \int_{\varphi_1}^{\varphi_2} \sin^2\varphi \,\mathrm{d}\varphi + 2G^*_{4,k} \int_{\varphi_1}^{\varphi_2} \sin^4\varphi \,\mathrm{d}\varphi .$$

Here φ_1 and φ_2 are the lower and upper bondaries of the given latitudinal zone (see Section 2). The variation of inclination of the Sun's axis is not yet taken into account. For each half-year interval we have three equations (for three zones) which must be solved in order to find N sets of coefficients G_0, G^*_2 and G^*_4.

The input data are arranged with respect to position angle. During a year, the (apparent) inclination of the Sun's axis changes, and the given value of the positional angle corresponds to different values of the latitude. We have calculated corrections, and the final formulae for each first half-year (January–June) look like:

$$G_2 = \frac{G^*_2}{0.99211054}, \quad G_4 = \frac{G^*_4}{0.98431522}$$

and for each second half-year (July–December):

$$G_2 = \frac{G^*_2}{0.99198754}, \quad G_4 = \frac{G^*_4}{0.98407076}$$

The next step is to construct the cubic spline interpolation with respect to the time variable, t, with the modification proposed by Kuklin and Stepanov (1983, see Appendix therein), where the fact that the observational data were really averaged, (integrated) over the latitudinal zone has been taken into account. Since the observational data are so arranged, we have modified the procedure of cubic spline approximation of these functions, and the boundary conditions for the spline were defined in the following way. We assumed that in the edge intervals (the first and last ones), the functions under consideration may be approximated with the same expressions as in the neighbouring intervals (the second and penultimate ones, respectively). Clearly, such a convention decreases the interpolation accuracy inside the edge intervals but it allows us to state the problem of the construction of spline interpolation in closed form.

The computations were made according to the following scheme.

(1) The forward process.

For each of the arrays of the coeffcients G_0, G_2, and G_4 we need to compute the arrays of p_k, z_k, and q_k values, where $1 \le k \le N-1$ and $\xi_k \equiv G^{(k)}_0$, $G^{(k)}_2$ or $G^{(k)}_4$; the starting values:

$$p_1 = \frac{1}{2}, \quad z_1 = 5\xi_2 + \xi_1, \quad q_1 = \frac{z_1}{4};$$

for $k = 2, \ldots, N-2$:

$$p_k = -\frac{1}{4 + p_{k-1}}, \quad z_k = 3(\xi_k + \xi_{k+1}), \quad q_k = p_k(q_{k-1} - z_k);$$

the finishing values:

$$p_{N-1} = 0, \quad z_{N-1} = 5\xi_{N-1} + \xi_n, \quad q_{N-1} = \frac{(z_{N-1}/2) - q_{N-2}}{2 + p_{N-2}}.$$

For all three sets of coefficients G_0, G_2, and G_4 the p_k values are the same, but z_k and q_k change.

(2) The backward process.

The y_k values ($1 \le k \le N-1$) are computed, where $y_k \equiv g_0^{(k)}$, $g_2^{(k)}$, and $g_4^{(k)}$ are instantaneous values of the coefficients in (2) in contrast to $G_0^{(k)}$, $G_2^{(k)}$, and $G_4^{(k)}$, averaged over a half-year:

$$y^{N-1} = q^{N-1}, \quad y_k = p_k y_{k+1} + q_k \quad (1 \le k \le N-2);$$

the boundary values:

$$y_0 = 8y_1 + 5y_2 - 12\xi_2, \quad y_N = 5y_{N-2} + 8y_{N-1} - 12\xi_{N-1};$$

interpolation in the middle of a half-year interval:

$$y_{k+1/2} = \frac{6\xi_k - y_k - p_{k+1}}{4}.$$

Over each interval, y is a quadratic polynomial of the time variable and is fully determined by the y_k, $y_{k+1/2}$, and y_{k+1} values. So, for interpolation in the middle of the intervals $[y_k, y_{k+1/2}]$ and $[y_{k+1/2}, y_{k+1}]$ have respectively:

$$y_{k+1/4} = \frac{3y_k + 6y_{k+1/2} - y_{k+1}}{8}, \quad y_{k+3/4} = \frac{-y_k + 6y_{k+1/2} + 3y_{k+1}}{8}.$$

Finally we have to construct isolines of C_1, separating areas occupied by different evolutionary regimes. Let the boundary value of the coefficient C_1^{XY} be given. Then we have the biquadratic equation for any time instant, t:

$$g_0(t) + g_2(t)\sin^2(t)\varphi + g^4(t)\sin\varphi = C_1^{XY}$$

or

$$g_4(t)\psi^2 + g_2(t)\psi + g_0(t) - C_1^{XY} - 0,$$

where $\psi = \sin^2\varphi$, and the roots of this equation satisfying $0 < \psi < 1$ must be found.

9 APPENDIX C

According to the modern scenario of the 11-year cycle of solar activity (Kuklin *et al.*, 1990) one can detect the following reference points on the cyclic curve of Wolf numbers: m – the minimum, t_{mA} - the beginning of the ascending phase, t_{AM} – the beginning of the maximum phase, M – the maximum, t_{MD} – the beginning of the descending phase, and t_{Dm} – the beginning of the minimum phase. The positions of these reference points in cycles 20 and 21 are presented in Table 1. The catalogue of turning points is given by Kuklin (1992).

Table 1.

Reference point	*Cycle 20*	*Cycle 21*
m	1964.625	1976.375
t_{mA}	1965.875	1977.585
t_{AM}	1967.250	1979.375
M	1968.875	1980.125
t_{MD}	1970.625	1981.875
t_{Dm}	1973.875	1985.125
m	1976.375	1986.625

Acknowledgements

The authors are grateful to Drs V. Rušin and M. Rybanský (Astronomical Institute of the Slovak Academy of Sciences) for permission to use unpublished observational data. Also we are obliged to Dr V. N. Obridko for discussions. This work was supported by the Russian Foundation for Basic Research NN 96-02-18383 and 96-02-16579.

References

Badalyan, O. G. and Kuklin, G. V. (1993) *Astron. Zh.*, **70**, 856.
Badalyan, O. G., Kuklin, G. V., and Kulčar L. (1993) *Solnechnye Dannye*, No. 8, 81.
Bumba V., Rušin, V., and Rybanský, M. (1990) *Bull. Astron. Inst. Czechosl.*, **41**, 253.
Girshik, M. A. (1936) *J. Amer. Stat. Ass.* **31**, 519.
Hoeksema, J. T. (1991) *Adv. Space Res.* **11**, No. 1, 15.
Hotelling, K. (1933) *J. Educ. Psychol.* **24**, 417; 498.
Karuhnen, K. (1947) *Ann. Acad. Sci. Fennicae* **A1**, No. 37, Helsinki, 3.
Kuklin, G. V. (1980) *Bull. Astron. Inst. Czechosl.* **31**, 224.
Kuklin, G. V. (1992) *Solnechnye Dannye* No. 10, 69.
Kuklin, G. V., Obridko, V. N., and Vitinsky, Yu. I. (1990) *Solar-Terrestrial Predictions*, Proc. Workshop Leura, Australia, 1989, Boulder, Colo. USA, 474.
Kuklin, G. V. and Stepanov, V. E. (1983) *Proc. of the 11th Reg. Conference on Solar Phys.*, Pt. 2, Debrecen., 389.
Leroy, J. L. and Noëns, J. C. (1987) *Astron. Astrophys.* **120**, L1.
Loewe, M. (1963) *Probability Theory* 3rd ed., Princeton University Press, Princeton, N.Y.
Obridko, V. and Gaziev, G. (1992) In: K. L. Harvey (ed.), *The Solar Cycle*, (ASP Conference Series, vol. 27), 410.
Pearson, K. (1901) *Phil. Mag.* **6**, 559.
Rao, C. R. (1965) *Linear Statistical Inference and Its Application*, Wiley. New York.
Rybanský, M. (1975) *Bull. Astron. Inst. Czechosl.* .**26**, 367.
Rybanský, M., Manik, K., and Rušin, V. (1985) *Contrib. Astron. Obs. Skalnaté Pleso* **13**, 127.
Rybanský, M., Rušin, V. and Dzifčáková, E. (1989) *Contrib. Astron. Obs. Skalnaté Pleso* **18**, 81; (1990) **19**, 193; (1991) **21**, 107.
Sýkora, J. (1980) *Bull. Astron. Inst. Czechosl.* **22**, 12.
Sýkora, J. (1980) In: M. Dryer and E. Tandberg-Hanssen (eds.), *Solar and Interplanetary Dynamics. IAU Symp* No. 91, 87.
Sýkora, J. (1992) *Contrib. Astron. Obs. Skalnaté Pleso* **22**, 55.
Sýkora, J. (1994) *Adv. Space Res.* **14**, No. 4, 73.

Storini, M. and Sýkora, J. (1997) *Sol. Phys.* **176**, 717.
Waldmeier, M. (1955) *Ergebnisse und Probleme der Sonnenforshung*, Leipzig, 313.
Wertlieb, A. B., Kopecký, M., and Kuklin G.V. (1971) *Issled. po Geomagn. Aeron. Fiz. Solntsa. Irkutsk* **2**, 194.
Wilks, S. S. (1962) *Mathematical Statistics*, Wiley, New York.